

On the Dynamics of Shock-Interface Interaction using the Level Set Method

A. Bagabir¹, A. Balabel², W. A. El-Askary^{2c}

¹Faculty of Engineering, Sana'a University,
P. O. Box 13282, Sana'a, Yemen

²Faculty of Engineering, Menofia University
Shebin Elkom, Menofia, Egypt

Received: 17/09/2010 – Revised 23/10/2010 – Accepted 08/11/2010

Abstract

The present work is concerned with the time accurate numerical solution of Euler equations coupled with the level set method to deal with the topological changes of the interface in compressible gas-gas flows due to an incident shock. The simulation is conducted by solving the unsteady compressible Euler equations along with the equation of state for an ideal gas. The scheme is implemented in conjunction with an implicit-unfactored method which is based on Newton-type sub-iterations and Gauss–Seidel relaxation and matrix preconditioning. The high-order flux reconstruction is an averaging procedure in which the flow variables and, subsequently the fluxes, are calculated at the cell faces by hybrid scheme. It is a combination of Riemann method and the modified Steger and Warming Flux Vector Splitting (FVS) method. The characteristics values at the cell faces are performed by a modified MUSCL scheme. The performance of the solver has been assessed through a series of numerical experiments of interaction of weak shock wave with cylindrical, sinusoidal and inclined interfaces separating two different gases. The present results, including numerical image, evolution of the interface, and growth rate behaviour, are seen to be in agreement with the available previous numerical and experimental data.

Keywords: Shock-interface interaction; Shock-bubble interaction; Level-set method; Gas-gas interface; Two-dimensional flow; Euler equations; Unsteady compressible flow.

1. Introduction

The problem of shock-interface interaction has received extensive attention over the last decades due its practical importance in compressible hydrodynamics. Common examples are the gas-bubble interaction problems (*e.g.* collapse of cavitation bubbles by incident shock) and shock–boundary layer interaction. The encountered flow phenomena in such cases can be seen in several practical flow problems, spanning from aerospace to medical engineering. Such multi-medium fluid flows give rise to challenging problems in both theory and numerical simulation.

Studies of shock-contact interactions are motivated by a desire to understand turbulent mixing in supersonic combustion ramjets whereby air and fuel can be mixed efficiently in the short transit times available, in inertial confinement fusion where mixing inhibits fusion, and in astrophysical phenomenon such as supernovae.

^c Corresponding Author: Wageeh Ahmed El-Askary

Email: wageeh_elaskary@yahoo.com Telephone: +20105255817

© 2009-2012 All rights reserved. ISSR Journals

PII: S2180-1363(10)24176-X

Although the numerical simulations of shock wave phenomena are now fairly commonplace, however, they are mostly restricted to single component flows. Unfortunately, multi-component extensions of successful single component schemes often suffer from spurious oscillations which are generated at material interfaces.

Several numerical methods have been applied extensively for the modeling of multi-component compressible flows. The methods that allow for the computation of the dynamics of the shock waves-moving interfaces interaction have received a great attention. These methods can be classified into either shock-capturing methods or front-tracking methods. Although both categories have been considerably improved, however, always yield a numerical diffusion and slight parasitic oscillations of moving interfaces, see for more details Cocchi and Saurel [1].

Eulerian schemes work well for most gas-gas interface problems and can efficiently handle large deformations of fluid interfaces. However, they can admit non-physical oscillations near fluid interfaces due to the smeared out density profile and the radical change in equation of state across fluid interfaces. Lagrangian schemes also work well on material interfaces, since they do not smear out the density profile and it is clear which equation of state is valid at each point. Unfortunately, Lagrangian schemes have their own problems when subjected to large deformations. Most numerical methods for interfacial flows are based on Eulerian schemes with embedded Lagrangian techniques.

The refraction of shock at a material interface has been previously studied both experimentally and numerically. Henderson et al. [2] have provided insight into the complex problem of anomalous refraction. Emphasis has been placed on the pattern of reflected and refracted waves, including precursors. However, the evolution of the interface itself is of considerable interest in problems ranging from inertial confinement fusion to astrophysics (Klein and Colella [3]) and has generated a flurry of activity that encompasses the subject of compressible turbulence. The basis for the study of the evolution of a shocked interface stems from the question of the Rayleigh-Taylor (RT) instability (Taylor [4]). The stability of an interface submitted to gravitational forces was investigated for the case in which the density of one of the materials across the interface was negligible compared to the other. Taylor [4] analyzed the case in which the Atwood number (ratio of the difference of the densities to their sum) is less than 1, and the acceleration of the system is constant. The interface was found to be unstable to small perturbations only if the direction of the acceleration normal to the interface coincides with that of the density gradient.

Richtmyer [5] extended Taylor's analysis to the case of an impulsive acceleration. His results implied that the interface would be unstable irrespective of the relative orientation of the velocity impulse and the density gradient. His predictions were verified experimentally by Meshkov [6], and the Richtmyer-Meshkov (RM) instability became a subject of research in its own right. Experimental, analytical and numerical studies performed by Rupert [7] clearly addressed this problem.

It was shown by Jenny et al. [8] and Karni [9, 10] that upwind conservative methods admit nonphysical oscillations near material interfaces. In Ref. [8], a conservative discretization of the calorically perfect Euler equations was shown to admit nonphysical oscillations when there is a jump in both temperature and specific heat ratio across an interface. They proposed non-conservative modifications of the conservative numerical method in regions where difficulties may occur. However, these modifications give rise to conservation errors in the total energy of the system, and thus yield a locally non-conservative formulation. In general, non-conservative formulations give the wrong shock speeds, although errors in shock speeds can be reduced significantly if the special viscosity term is added [11].

The approach introduced by Karni [10, 11] is to solve the Euler equations separately on each side of the interface using a method designed for a single-component flow, while the interface is dealt within a different manner using an evolution equation derived from the energy equation. Despite the fact that the method is not exactly conservative at the interface, reasonable results were obtained using this approach in conjunction with either standard level-set or mass-fraction

formulation of ideal gases, see [12]. Qamar and Warnecke [13] simulated multi-component flows using high order central schemes. They introduced numerical methods for the conservative extension of the classical Euler equations to multi-component flows. High-resolution central schemes were used to solve these equations. The equilibrium states for each component were coupled in space and time to have a common temperature and velocity. Usually conservative Euler solvers for the gas mixtures produce nonphysical oscillations near contact discontinuities, if the temperature and the ratio of specific heats both are not constant there. However, Qamar and Warnecke [13] considered in the schemes that the oscillations near the interfaces are negligible. The schemes also guaranteed the exact mass conservation for each component and the exact conservation of total momentum and energy in the whole particle system. The central schemes were robust, reliable, compact and easy to implement. Several one- and two-dimensional numerical test cases, such as shock helium bubble and shock R22 bubble interactions, were included in the paper of Qamar and Warnecke [13], which validated the application of these schemes to multi-component flows. However, Qamar and Warnecke [13] found through their numerical experiments that pressure and velocity fluctuations near gas interfaces are very small and do not seem to interfere with the physics of the simulation. The reason of these small fluctuations is the presence of sufficient implicit numerical dissipation in the central schemes which allows smooth shocks transition. For more detail regarding numerical dissipation and numerical shock instability, see Xu [14].

Quirk and Karni [15] presented a detailed numerical study of the interaction of a weak shock wave with an isolated cylindrical gas inhomogeneity. Such interactions have been studied experimentally in an attempt to elucidate the mechanisms whereby shock waves propagating through random media enhance mixing. The study concentrated on the early phases of the interaction process which are dominated by repeated refractions and reflections of acoustic fronts at the bubble interface. Specifically, Quirk and Karni [15] have reproduced two of the experiments performed by Haas and Sturtevant [16]: at Mach=1.2 a planar shock wave moving through air, impinging on a cylindrical bubble which contains either helium or Refrigerant 22. These flows are modeled using the two-dimensional compressible Euler equations for a two component fluid (air-helium or air-Refrigerant). In order to avoid the spurious oscillations generated at material interfaces, Quirk and Karni [15] have employed a novel non-conservative shock-capturing scheme. In addition, they have utilized a sophisticated adaptive mesh refinement algorithm which enables extremely high resolution simulations to be performed relatively cheaply. Thus Quirk and Karni [15] have been able to reproduce numerically all the intricate mechanisms that were observed experimentally (e.g. transition from regular to irregular refraction-cusp formation and shock wave focusing, multi shock and Mach shock structures, jet formation etc.). Moreover, Quirk and Karni [15] could present an updated description for the dynamics of a shock-bubble interaction.

Both Picone and Boris [17] and Yang et al. [18] have performed computations aimed at determining the long-time evolution of the bubble inhomogeneities, while Loehner et al. [19] have investigated the early-time dynamics of the interaction process. All these numerical studies were performed according to the experimental data of Haas and Sturtevant's experiments [16]. However, in these studies the flow was modeled using a single gas rather than the exact binary system used by the experiment. This simplification, whilst expedient, inevitably reduced the accuracy of the results. Note that since some desired density jump must be imposed across the bubble interface with a single gas component model the bubble cannot be in thermal equilibrium with its surroundings as was the case with the experiments.

In a more recent study, Large-eddy simulation of multi-component compressible turbulent flows using high resolution methods was performed by Thornber et al. [20]. They examined the ability of a finite volume Godunov and a semi-Lagrangian large-eddy simulation (LES) method to predict shock induced turbulent mixing through different simulations. Thornber et al. [20] concluded that very good agreement was gained in qualitative comparisons with experimental results for combined Richtmyer–Meshkov and Kelvin–Helmholtz instabilities in compressible turbulent multi-component flows. It was also shown that both numerical methods can capture the

size, location and temporal growth of the main flow features. In comparing the methods, there was variability in the amount of resolved turbulent kinetic energy. The semi-Lagrangian method had constant dissipation at low Mach number, thus allowing the initially small perturbations to develop into Kelvin–Helmholtz instabilities. These were suppressed at the low Mach stage in the Godunov method. However, Thornber et al. [20] found that there was an excellent agreement in the final amount of fluid mixing when comparing both numerical methods at different grid resolutions. However, LES requires a huge storage memory and supercomputers and of course very expensive to be used, see El-Askary [21].

Recently, a level set formulation for tracking moving interfaces in compressible gas dynamics has been introduced, Mulder et al. [22]. This algorithm can handle the complex topological changes such as merging and breaking of interfaces with no special treatment. In the level set methods the interface is represented as the zero level set of a smooth function G defined on the entire physical domain and satisfying a transport equation. It presents several advantages: there is no need to reconstruct the interface or to re-grid the neighbourhood of the discontinuity. Moreover, it can be easily generalized to three dimensions.

The main application of level set method is to track evolving topological changes of interface separating different fluids. This is done by viewing the interfacial boundary as an interface, and then using the method to keep track of the boundary. Mulder et al. [22] early attempted to couple level set methods to the problem of fluids with compressible fluid flows. Euler equations with the equation of state for an ideal gas were used. A sharp interface was assumed, which separated gases with two different adiabatic exponents, and the Euler equations were amended to include a level set equation written in conservation form. Karni [23] showed that this algorithm produces unphysical oscillations. She attributed such oscillations to the discretization applied in the conservation form that failed to give the correct jump conditions at the interface between the two gases. In the case of the compressible Euler equation, the pressure should be continuous at the interface; however, any discrete conservative formulation will disrupt this jump condition and cause oscillations [24]. To eliminate these oscillations, Karni [23] did not consider the conservative form of the finite-difference scheme at the interface between the two gases. The conservation form was maintained elsewhere, thus ensuring that shock waves will be computed correctly. Quirk and Karni [15] used this solver to compute the interaction of a shock wave in air with a helium bubble.

More recently, an adaptive ghost fluid finite volume numerical method has been developed by Wang et al. [25] and applied for compressible gas-water flow problems. This method could predict several gas-water flow problems involving large gradient density at the interface and strong shock-interface interaction. This work showed that the local mesh clustering in the vicinity of the interface can effectively reduce both numerical and conservative errors caused by the standard ghost fluid method. Although good results have been obtained by this method for one- and two-dimensional multi-medium flows, however, it is expected that such numerical methods are extremely computationally demanding for three-dimensional flow problems.

Given this background, the purpose of the present study is to explore the extent to which a modern computational method could complement the experiments of Haas and Sturtevant [16] and the numerical study performed by Quirk and Karni [15] in elucidating the basic mechanisms that govern the propagation of shocks through non-uniform gases. Additionally, it is thought that such a study could help bridge the gap between existing theories of shock reflection-refraction phenomena and experiment. For example, although Haas and Sturtevant [16] were able to use the theory of geometrical acoustics to gain a good understanding of their experimental observations, this theory ignores wave nonlinearities and so it fails to account for all flow features. The present computational study tries to avoid the above shortcomings, discussed in the literature. First, proper account is taken of the separate gas components; the flow is modeled by the compressible Euler equations for a two-component fluid (air-helium or air-Refrigerant 22 (R22) depending upon the experiment being simulated). Although this represents a small generalization over the single component case, most popular shock-capturing schemes do not perform satisfactorily for multi-

component flows in that they produce spurious oscillations at material interfaces (e.g. Abgrall [26]). Since such numerical artifacts can have a significant effect upon the evolution of a material interface, they are to be avoided. Here we employ a somewhat novel technique to avoid this numerical difficulty. In essence, the scheme allows for a controlled conservation error so as to maintain the correct pressure equilibrium between different fluid components. While this relaxation of strict conservation runs against perceived wisdom in the design of numerical schemes for flows with shock waves (Lax [27, 28]), it does produce good results. Second, we overcome the shortcoming of poor resolution by utilizing a sophisticated adaptive mesh refinement scheme (Quirk [29]). This scheme can reduce by several hundred-fold the cost of performing detailed simulations and so it allows for simulations that would otherwise prove to be prohibitively expensive. The level set method is applied for tracking the sharp interface between the compressible gases. The initial data is smoothed by assigning modified area-weighted values to the appropriate cells to avoid the staircase configuration of the data. Moreover, after advection the sharp interface, a reinitialization of the level set function on the computational field is applied. A further verification to the present scheme is introduced through the comparisons with the experiment of Benjamin et al. [30] and the numerical studies of Zhang and Sohn [31] and Weaver et al. [32]. The present study is extended to include a simulation of inclined interface separating air and He with the presence of an attacking shock wave.

2. Numerical details

2.1. Governing equations

The computational code used in the present study is based on the finite volume solver for the solution of the Euler equations for compressible flow. The two-dimensional Euler equations can be written in matrix form and curvilinear coordinates as:

$$\frac{\partial Q}{\partial T} + \frac{\partial F_\xi}{\partial \xi} + \frac{\partial F_\zeta}{\partial \zeta} = 0$$

(1)

where T is time and F is the inviscid flux, which can be written as:

$$F_\xi = J \begin{pmatrix} \rho \tilde{U} \\ \rho u \tilde{U} + p \xi_x \\ \rho w \tilde{U} + p \xi_z \\ (e + p) \tilde{U} \end{pmatrix}, \quad F_\zeta = J \begin{pmatrix} \rho \tilde{W} \\ \rho u \tilde{W} + p \zeta_x \\ \rho w \tilde{W} + p \zeta_z \\ (e + p) \tilde{W} \end{pmatrix} \quad (2)$$

with the contravariant velocities defined as:

$$\tilde{U} = u \xi_x + w \xi_z, \quad \tilde{W} = u \zeta_x + w \zeta_z \quad (3)$$

The conservative variable, Q , is given by:

$$Q = J(\rho, \rho u, \rho v, e)^T = JU^T \quad (4)$$

where ρ is the density, u and v are the velocity components, and e is the total energy per unit volume. J stands for the Jacobian of the transformation from Cartesian (x, z) to curvilinear (ξ, ζ) coordinates.

The pressure, p , is calculated by the perfect gas equation of state, $p = \rho(\gamma - 1)i$, where γ is the ratio of specific heats (for air $\gamma_{\text{air}} = 1.4$) and i is the specific internal energy.

The advective flux derivative $\frac{\partial F_\xi}{\partial \xi}$ (similarly for $\frac{\partial F_\zeta}{\partial \zeta}$) is discretised at the centres of the control volumes (i, j) generated by the grid using the values of the intercell fluxes, e.g., $\frac{\partial F_\xi}{\partial \xi} = \frac{F_\xi(j+1/2, k) - F_\xi(j-1/2, k)}{\Delta \xi}$, where $\Delta \xi = \Delta \zeta = 1$ in the transformed computational domain. The determination of the intercell flux function is the main aim of the numerical scheme.

2.2. Numerical scheme

One of the challenges in the numerical simulations is to eliminate the numerical dissipation which may be responsible for suppressing the flow-field details. Therefore, the investigation has been performed using high resolution hybrid scheme which was used in the past for the study of various compressible flows [33, 34, 35]. The hybrid scheme is a combination of Riemann method [36] and the modified Steger and Warming Flux Vector Splitting (*FVS*) method [37]. The Riemann method contains an approximate solution of the local Riemann problem at the cell faces, whereas the *FVS* scheme splits the flux terms into a left and a right part and discretises them according to the sign of the associated propagation speeds. Generally speaking, the *FVS* scheme is simpler in the formulation and more efficient in the implementation but it poses a higher numerical dissipation that prohibits sharp or accurate resolution of discontinuities and shear layers.

According to the hybrid scheme, the inviscid flux, F , at the cell faces of the control volume $(j+1/2)$ is given by [36, 38]:

$$F_{j+1/2} = \phi F_{FVS} + (1 - \phi) F_{Riemann} \quad (5)$$

The fluxes F_{FVS} and $F_{Riemann}$ are calculated by *FVS* method and the Riemann method, respectively. The *FVS* flux can be computed as:

$$F_{FVS} = F^+(U_L) + F^-(U_R), \quad (6)$$

Where,

$$F^\pm = \rho J |\nabla \xi| \begin{pmatrix} \frac{1}{2}(\lambda_1^\pm + \lambda_2^\pm) \\ \left(u + \frac{S \xi_x / |\nabla \xi|}{\gamma}\right) \frac{\lambda_1^\pm}{2} + \left(u - \frac{S \xi_x / |\nabla \xi|}{\gamma}\right) \frac{\lambda_2^\pm}{2} \\ \left(w + \frac{S \xi_z / |\nabla \xi|}{\gamma}\right) \frac{\lambda_1^\pm}{2} + \left(w - \frac{S \xi_z / |\nabla \xi|}{\gamma}\right) \frac{\lambda_2^\pm}{2} \\ \frac{1}{2} \left(\frac{e+p}{\rho}\right)^\pm (\lambda_1^\pm + \lambda_2^\pm) \end{pmatrix} \quad (7)$$

where S is the sound speed and $|\nabla \xi| = \sqrt{\xi_x^2 + \xi_z^2}$. The variable U_L and U_R are intercell values of the conservative variables. The split eigenvalues λ_1^\pm and λ_2^\pm are defined by:

$$\lambda_1^\pm = \frac{\lambda_1 \pm |\lambda_1|}{2} \quad \text{with } \lambda_1 = \lambda_o + S \quad (8)$$

$$\lambda_2^\pm = \frac{\lambda_2 \pm |\lambda_2|}{2} \quad \text{with } \lambda_2 = \lambda_o - S \quad (9)$$

where

$$\lambda_o = u\xi_x + w\xi_z \tag{10}$$

The Riemann flux is given by:

$$F_{Riemann} = J \begin{pmatrix} \overline{\rho u \xi_x + \rho w \xi_z} \\ \overline{\rho u (\rho u \xi_x + \rho w \xi_z) / \rho + p \xi_x} \\ \overline{\rho w (\rho u \xi_x + \rho w \xi_z) / \rho + p \xi_z} \\ \overline{(e + p)(\rho u \xi_x + \rho w \xi_z) / \rho} \end{pmatrix} \tag{11}$$

The variables $\overline{\rho}$, $\overline{\rho u}$, $\overline{\rho w}$ and \overline{e} are defined in Bagabir and Drikakis [35] as:

$$\overline{\rho} = \rho_0 + r_1 + r_2 \tag{12}$$

$$\overline{\rho u} = (\rho u)_0 + (u + S\xi_x)r_1 + (u - S\xi_x)r_2 \tag{13}$$

$$\overline{\rho w} = (\rho w)_0 + (w + S\xi_z)r_1 + (w - S\xi_z)r_2 \tag{14}$$

$$\overline{e} = e_0 + \left(\frac{e+p}{\rho} + S\lambda_o\right)r_1 + \left(\frac{e+p}{\rho} - S\lambda_o\right)r_2 \tag{15}$$

$$\begin{aligned} r_1 = \frac{1}{S^2} & \left\{ \left[\frac{\gamma-1}{2}(u^2 + w^2) - S\lambda_o \right] \frac{(\rho_1 - \rho_0)}{2} \right. \\ & + \left[S \frac{\xi_x}{\nabla \xi} - (\gamma-1)u \right] \frac{[(\rho u)_1 - (\rho u)_0]}{2} \\ & + \left[S \frac{\xi_z}{\nabla \xi} - (\gamma-1)w \right] \frac{[(\rho w)_1 - (\rho w)_0]}{2} \\ & \left. + \frac{(\gamma-1)(e_1 - e_0)}{2} \right\} \end{aligned} \tag{16}$$

$$\begin{aligned} r_2 = \frac{1}{S^2} & \left\{ \left[\frac{\gamma-1}{2}(u^2 + w^2) - S\lambda_o \right] \frac{(\rho_2 - \rho_0)}{2} \right. \\ & + \left[S \frac{\xi_x}{\nabla \xi} - (\gamma-1)u \right] \frac{[(\rho u)_2 - (\rho u)_0]}{2} \\ & + \left[S \frac{\xi_z}{\nabla \xi} - (\gamma-1)w \right] \frac{[(\rho w)_2 - (\rho w)_0]}{2} \\ & \left. + \frac{(\gamma-1)(e_2 - e_0)}{2} \right\} \end{aligned} \tag{17}$$

The variables Ψ_l ($\Psi = \rho, \rho u, \rho w, e, l = 0,1,2$) are the values on the three characteristics and can be computed from:

$$\Psi_l = \frac{1}{2} \left([1 + \text{sign}(\lambda_l)]U_L + [1 - \text{sign}(\lambda_l)]U_R \right) \tag{18}$$

where, the left U_L and the right U_R states of the conservative variables are calculated via the MUSCL scheme.

The introduction of the *FVS* scheme is required in the case of supersonic Mach numbers where the Riemann solver does not provide sufficient numerical dissipation to capture strong shock waves. The limiter ϕ is given by [38]:

$$\phi = \min \left(1, a \left(1 - \min(f_j, f_{j+1}) \right) \left| M_{j+1} - M_j \right|^2 \right) \tag{19}$$

The coefficient a takes the value of 2 in supersonic flows, and M is the local Mach number. The flux limiter f like that of van Albada [39] can be used to suppress oscillations near discontinuities and extrema by locally reducing the order of the reconstruction to first order:

$$f_j = \max\left(0, \frac{2\nabla U_j \Delta U_j}{(\nabla U_j)^2 + (\Delta U_j)^2 + \varepsilon}\right) \quad (20)$$

Where, $\nabla U_j = U_j - U_{j-1}$ and $\Delta U_j = U_{j+1} - U_j$, and ε is a small positive number preventing division by zero.

To obtain higher-order accuracy the modified MUSCL-approach according to Thomas et al. [40] has been employed for calculating the conservative variables at the cell faces of the control volumes. In this approach a set of variables is extrapolated from both sides to the cell interface. With these values a common numerical flux is formulated. A conservative variable U is interpolated at the cell face $j+1/2$ as follows:

$$U_L = U_j + \frac{g_j}{4} [(1 - kg_j)\nabla U_j + (1 + kg_j)\Delta U_j] \quad (21)$$

$$U_R = U_{j+1} + \frac{g_{j+1}}{4} [(1 + kg_{j+1})\nabla U_{j+1} + (1 - kg_{j+1})\Delta U_{j+1}] \quad (22)$$

The limiter g_j is a sensor function, modified form of the van Albada limiter, aiming at preventing spurious oscillations by reducing the accuracy of the scheme to first order in the vicinity of shock waves

$$g_j = 1 - [(1 - \eta f_j)(1 - f_j)^n] \quad (23)$$

where $n > 2$ is used for sharpening the limiter in the regions with strong discontinuities. Different interpolation schemes can be derived by using different values for the parameter k : fully upwind for $k = -1$, and centred for $k = 1$.

The time integration of the unsteady Euler equations has been obtained by the implicit-unfactored method second-order in time [34, 35, 41]. However, the time integration method is clearly explained in [35] and it is not necessary to repeat it here again.

2.3. Level Set Method

The level set method is a means for computing of the interface motion between two different fluids. In the level set formulation, the interface Γ is the zero level set of a smooth function G [42]:

$$\Gamma = \{x : G(x, T) = 0\} \quad (24)$$

Consequently, it can simply be defined as the areas where $G > 0$ are occupied by air, whereas areas with $G < 0$ are occupied by gas:

$$G(x, T) = \begin{cases} > 0 & \text{if } x \in \text{air} \\ = 0 & \text{if } x \in \Gamma \text{ (interface)} \\ < 0 & \text{if } x \in \text{gas} \end{cases} \quad (25)$$

The unit normal n on the interface and the curvature of the interface κ can easily be expressed in terms of the function G :

$$\mathbf{n} = -\frac{\nabla G}{|\nabla G|}, \quad \kappa = \nabla \cdot \mathbf{n} \quad (26)$$

The basic idea of the level set method is based on the advection of the interface with its local velocity vector, \mathbf{u} , through the solution of the simple hyperbolic equation [42]:

$$G_t + \mathbf{u} \cdot \nabla G = 0 \quad (27)$$

In order to ensure that the level set function stays well-behaved, it must be maintained as a distance function for all time [42]. That can be achieved through the fulfilment of the Eikonal equation, i.e. $|\nabla G|=1$. The satisfying of the Eikonal equation in the computational domain is known as reinitialization of the level set. Many reinitialization algorithms have been recently proposed. The reinitialization algorithm proposed by Sussman et al. [43] is used in the present paper for its efficiency and simplicity. Many numerical techniques have been adopted to solve the level set transport equation (27), as described in Sethian [42]. The different developed schemes showed an important effect on the stability of the solution. Recently, Balabel *et al.* [44] have developed a numerical method with high effectiveness and accuracy in obtaining the physical solution of some standard level set cases. This numerical method is based on the two step Runge-Kutta method for approximating the temporal advection, and the central difference for the discretization of the convective terms. In general, the present numerical method is based on the solution of the Euler equation for the velocity field on both sides of the interface separating two different gases. This velocity field is used to bring the interface to the new form and position via level set method. The computational domain is then reinitialized. Done in this manner, the method conserves mass to a large extent.

The central difference approximation, applied in the present paper, provides a high order accurate solver compared with the first order upwind scheme used in all the previous level set numerical methods. However, the original work of Sethian [45] has showed that the central difference is failed in two specified cases; namely; the movement of a V-front under a dependent gradient normal speed and the movement of a cosine curve under a normal speed along it normal vector field. The central difference approximation produces in such cases a miscalculation at the junction point of the V-front, which propagates outwards as wild oscillation. These oscillations cause blow-up in the code. It should be pointed that these miscalculations have nothing to do with the computational grid distance or the definite time step. Accordingly, Sethian [45], has concluded that more attention should be given for the gradient term discretization of ∇G in a way that correctly accounts for the entropy condition. Following that, the majority of the papers concerned with the development of the level set technique have applied different upwind schemes for solving the level set equation ranging from first-order to second-order ENO or fifth-order WENO scheme. Therefore, we have to perform the specified cases as an important test for our proposed algorithm.

Case I:

The initial configuration of The V-front initial is a "V" formed by rays meeting at (0.5, 0) and can be given by:

$$G(x,0) = \begin{cases} \frac{1}{2} - x & \text{if } x \leq \frac{1}{2} \\ x - \frac{1}{2} & \text{if } x > \frac{1}{2} \end{cases} \quad (28)$$

The equation of motion for this case is given by:

$$G_t = F \sqrt{1 + G_x^2} \quad (29)$$

Consider F equals 1 for initial value problem and the difference numerical approximation of the temporal and the spatial derivative is given by:

$$G_t = \frac{G_j^{n+1} - G_j^n}{\Delta t} = \sqrt{1 + \left(\frac{G_{j+1}^n - G_{j-1}^n}{2\Delta x} \right)^2} \quad (30)$$

The expected problem due to central approximation of the gradient term is at $x=0.5$, where the slope is not defined. In the exact solution, $G_t = \sqrt{2}$ for all $x \neq 0.5$, and this should also hold

at $x=0.5$. However, from Eq.(30) we get the value 1. The Huyghen's construction proposed by Sethian [45] sets the correct value for G at $x=0.5$. Instead of that, we use the reinitialization process to reconstruct the level set according to the other correct values where $x \neq 0.5$ after each time step. Consequently, the value at the middle is reconstructed correctly. Fig. (1-a) shows the exact solution of the problem. Fig.(1-b) shows the calculated results using the central difference without reinitialization and the appearance of the miscalculation at $x=0.5$ can be seen. The miscalculation of G at $x=0.5$ is then spread over a wide range in successive time steps. Fig.(1-c) shows the calculated results using the central difference approximation with the reinitialization process. It can be observed that as a result of the reinitialization process, the miscalculations disappear. The reconstructive strength of the reinitialization process also holds, when cups with different forms are formed during other front evolution processes, as follows next.

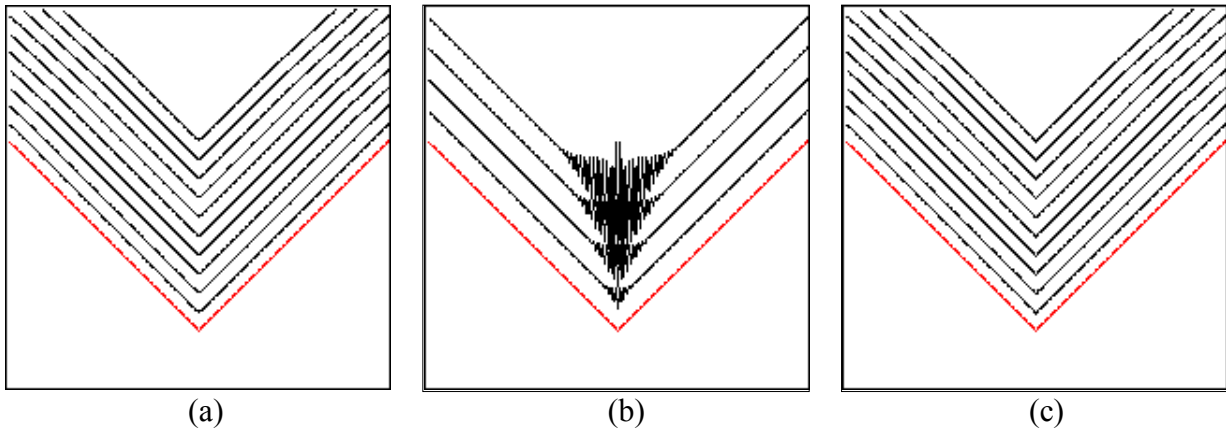


Figure 1 The advection of a "V"-front using the central difference approximation for the level set function, (a) the exact solution, (b) without reinitialization, (c) with the reinitialization

Case II:

The second case that shows the effectiveness of the proposed algorithm is the propagation of an initially simple and smooth cosine curve along its normal vector field with a normal speed $V_n=1.0$. As seen in Sethian [45], the front develops a sharp corner in finite time, and consequently, it is difficult to continue the evolution as the normal vector is ambiguously defined. By using the central difference scheme along with the reinitialization process, the front forms a cusp but the evolution is continued without any disturbances, as seen in Fig.(2).

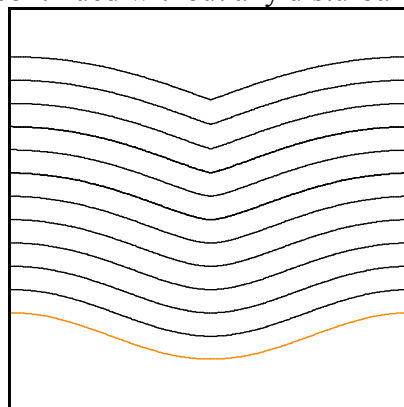


Figure 2 The advection of smooth cosine curve along its normal

2.4. Interface Boundary Conditions

In order to obtain a numerical method that can track the interface separating two different materials, one must specify accurately the boundary conditions at the interface. Since the interface can be considered as a contact discontinuity, moving with the normal local velocity V_n ,

the Rankine-Hugoniot jump conditions imply that $[p]=0$ and $[V_n]=0$: i.e. both the pressure and the normal velocity are continuous across the interface.

3. Results and discussion

The performance of the solver has been assessed through a series of numerical experiments of interaction of weak shock wave with cylindrical, sinusoidal and inclined interfaces separating two gases. The test cases are conducted in a rectangular shock tube. The boundary conditions are considered as followings:

- The left boundary corresponds to the region behind the shock wave obtained by the Rankine-Hugoniot relations.
- The right boundary was considered to permit smooth outflow of any rightward-moving waves by maintaining a zero-gradient condition for all variables.
- The upper boundary of the domain is the wall of the shock tube which treated as perfectly reflecting.
- The lower boundary of the domain could be either wall or symmetry condition depending on the case considered.

3.1 Cylindrical interface

The problem setup is similar to the experiment of Haas and Sturtevant [16]. Figure 3 shows a schematic of the computational domain with the initial conditions. A planar shock wave of Mach number $M = 1.2$ impinges on a cylindrical bubble. The shock propagates through air from the left to the right side of the shock tube. The cylindrical bubble has a radius of 25mm and the vertical dimension of the shock tube is 89mm . The horizontal dimension of the shock tube is 10 times the radius of the bubble. The bubble contains either helium (*He*) or Refrigerant 22 (*R22*). The *He*-gas bubble is lighter than the surrounding air ($\rho_{He}/\rho_{air} = 0.166$), while the *R22*-gas bubble is denser than the surrounding air ($\rho_{R22}/\rho_{air} = 2.86$). Unshocked pressure in both gases is 1.0 bar. The ratios of specific heats are $\gamma_{He} = 1.67$ and $\gamma_{R22} = 1.249$. It was found that the two configurations of the light and dense bubbles lead to a different interface evolution and flow behaviour [16, 33].

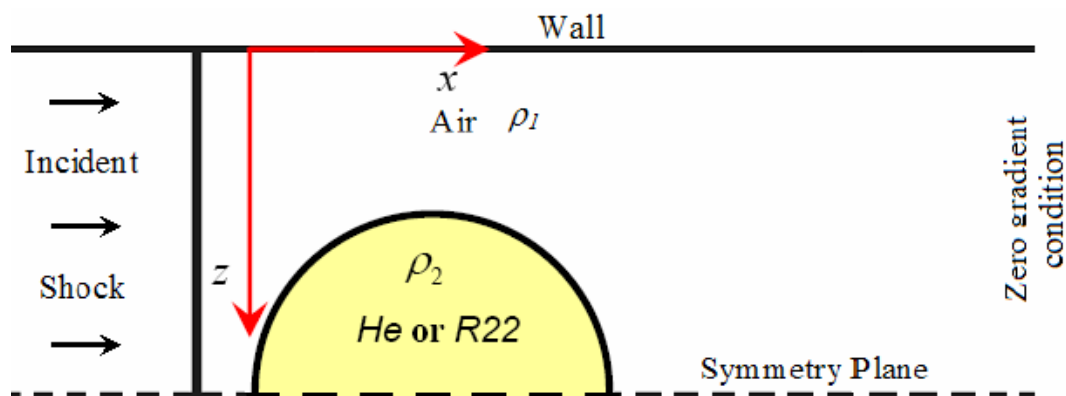


Figure 3 Schematic of computational domain of the cylindrical interface

The flow field is assumed to be symmetric about the axis of the shock tube and so only the top half of the flow field is computed. However, the numerical images are reconstructed about the symmetry plane to aid in visualisation. The numerical experiments is performed using Cartesian grid of 500×100 cells. This yields that the radius of bubble is represented by about 56 cells. Numerical experiments confirmed that the above grid resolution is sufficient to obtain grid-independent results [33]. The initial data is smoothed by assigning modified area-weighted values to the appropriate cells to avoid the staircase configuration of the data. Figure 4

demonstrates the effect of the initial data smoothing in both *He*- and *R22*-bubble interfaces at early and late evolution. The results without initial data smoothing (Fig. 4a) exhibit abnormal ripples, shown in dotted circles, at the upstream and downstream interface of the light bubble (top frames) and at the upstream interface of the dense bubble (bottom frames). The ripples are more pronounced at late interface evolution. These ripples disappear by removing staircase construction of the initial data as shown in Fig. 4b.

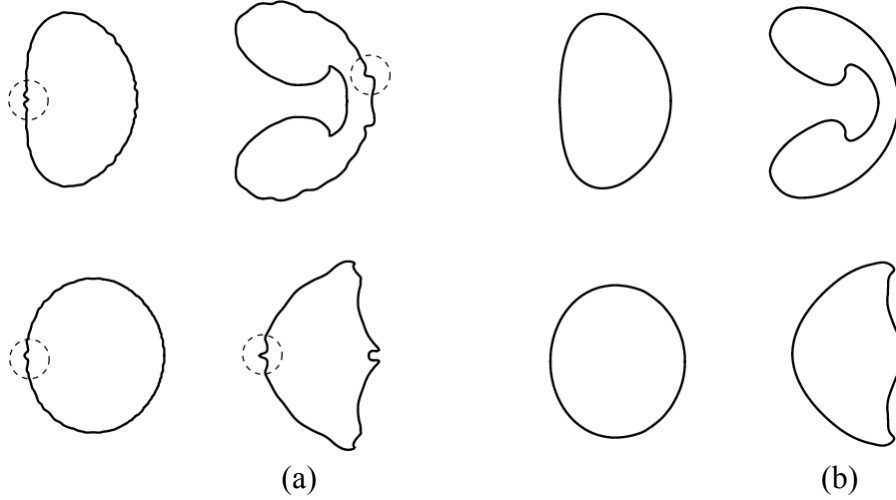


Figure 4 The effect of the initial data smoothing in *He* (top) and *R22* (bottom) bubble interfaces at early and late times (a) Without data smoothing. (b) With data smoothing

Computations are firstly performed for the interaction of the shock wave at $M = 1.2$ with the *He*-gas bubble. Figure 5 shows the numerical images and interfaces of the bubble for a sequence of time. The normalised time, t , is given by $t = \frac{T}{r/S}$, where S , r and T are the sound speed in the

ambient air, radius of the bubble and real time, respectively. The normalised time $t=0$ corresponds to the first collision of the shock wave with the bubble. It takes about one normalised time (corresponding to 61.8×10^{-6} seconds) for the incident shock to pass through a distance equals to the radius of the cylindrical bubble.

The first frame is at time $t=0.9$, in which the incident shock appears as two straight branches connected to curved reflected and refracted (inside the bubble) waves. The incident shock is just about halfway across the bubble. The refracted wave moves faster than the incident shock due to the higher speed of sound inside the bubble. The shock system exhibits twin regular reflection-refraction, *TRR* [2]. The refracted wave connects at the interface to two branches of the transmitted waves which cross the two branches of the incident shock and join the reflected wave. The air-*He* (upstream) interface deforms while the *He*-air (downstream) interface remains nearly unaffected. At $t=2.1$, the Mach stem of the incident shock is passing over the interface and the refracted wave transmits entirely from the bubble. Also, the numerical images depicts secondary transmitted wave. There are two waves reflected from the walls moving towards the centre of the shock tube. The upstream interface is almost flattened and the downstream interface starts to deform. It is also observed that the interface expands laterally. The third frame ($t=4.6$) shows remarkable motion to the downstream and deformation of the whole bubble interface. The bubble acquires a kidney shape. The upstream interface approaches the downstream interface. This is attributed to the formation of a central air jet at the middle of the bubble. As time goes on ($t=8.6$), the bubble continues to deform. The subsequent frames of Fig. 5 show the growth of the central jet by drawing fresh unmixed air towards the bubble interface. Subsequently, the bubble splits in two parts ($t=12.6$). As shown in the interface evolution ($t=8.6$), the air jet expands laterally and forms two circular-vortical structures. The vortical structures grow up and interact with the upper and lower sides of the bubble. Accordingly, as

seen from interface evolution at $t=12.6$, the upper and lower interfaces are penetrated by new formed jets. This may lead to splitting the bubble in four parts if the simulation is carried on to about time $t=26$.

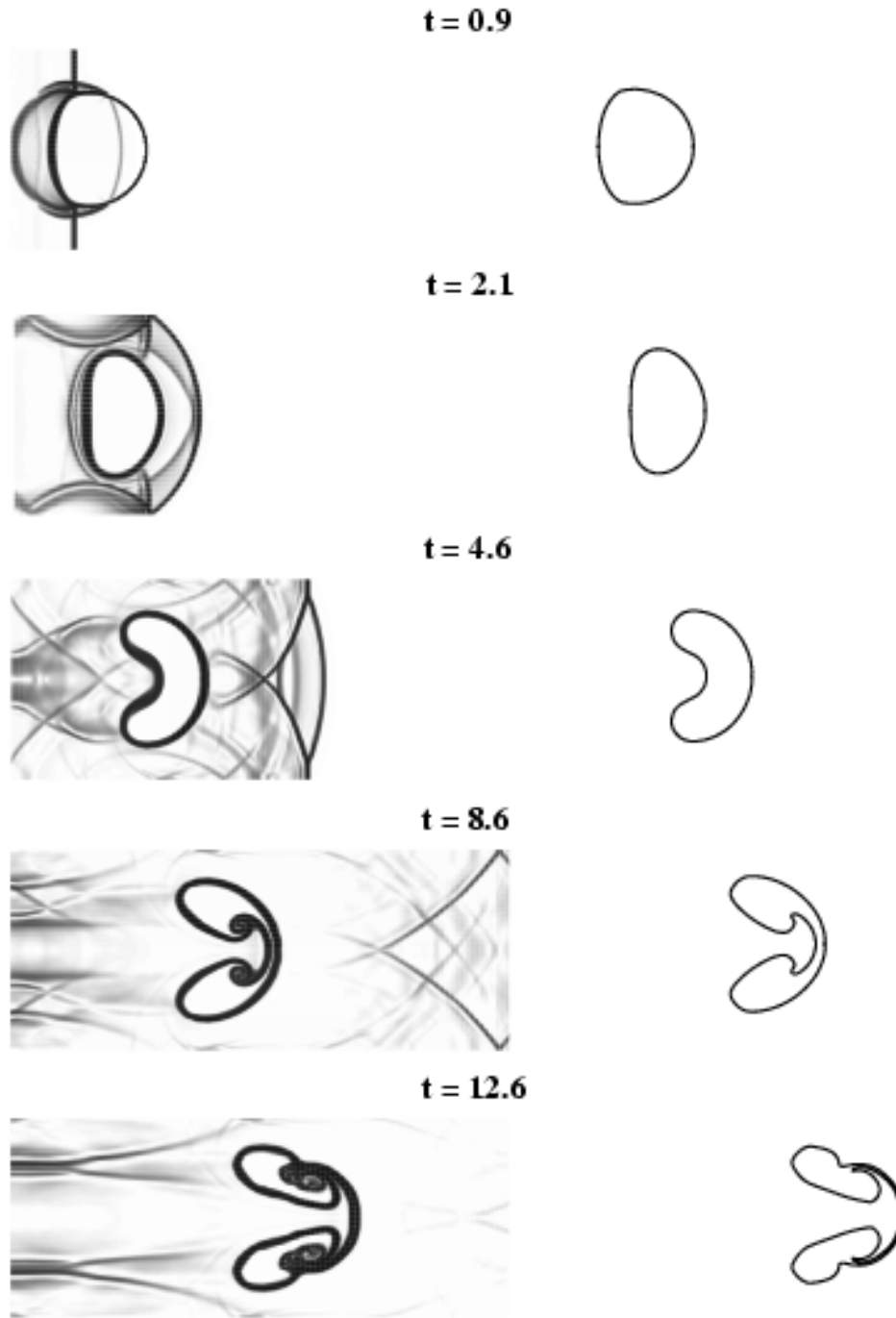


Figure 5 Normalized time sequence of numerical image (left) and interface (right) for $M = 1.2$ shock interaction with He bubble

Figure 6 shows the frames of the numerical image and interface of the interaction of a shock wave at $M=1.2$ with $R22$ bubble for a sequence of time. The first frame ($t=0.9$), depicts the initial stage of the interaction of the shock wave with low sound-speed gas. The shock system forms a regular reflection, RR . The incident and reflected shock waves appear outside the bubble and the convergent refracted shock exists inside. The convergent-refracted wave moves inside the bubble. It lies behind the incident shock because the sound speed inside the bubble is lower than that outside the bubble. The upstream interface starts to deform. The subsequent frame ($t=2.4$) shows the incident shock diffracted downstream and connected to the refracted wave. Although the bubble size gets smaller by shock compression, the downstream interface

has not yet undergone any deformation. The frame captures the reflected waves from the shock-tube walls. At time $t=4.6$, the incident shock moves away from the bubble but its tail is intact to the bubble interface. The two branches of the incident shock intersect. The dense bubble reinforces the refracted wave. This leads to high velocity, created by the transmitted shock at its focus, subsequently, forms a narrow axial jet on the downstream interface (as shown at $t=9.4$). As time goes on, the cylindrical bubble grows laterally due to the formation and growth of the vortex pairs. Moreover, the structure deforms into a large vortex and grows laterally during the formation of the vortices. The vortices grow in size by entraining the air left at the downstream side. This overtakes the forward-moving axial jet. It is noticed that the intact tail of incident shock is still existed. Moreover, the frames illustrate many reflected waves, shock-shock interactions and shock focusing events occur inside the bubble.

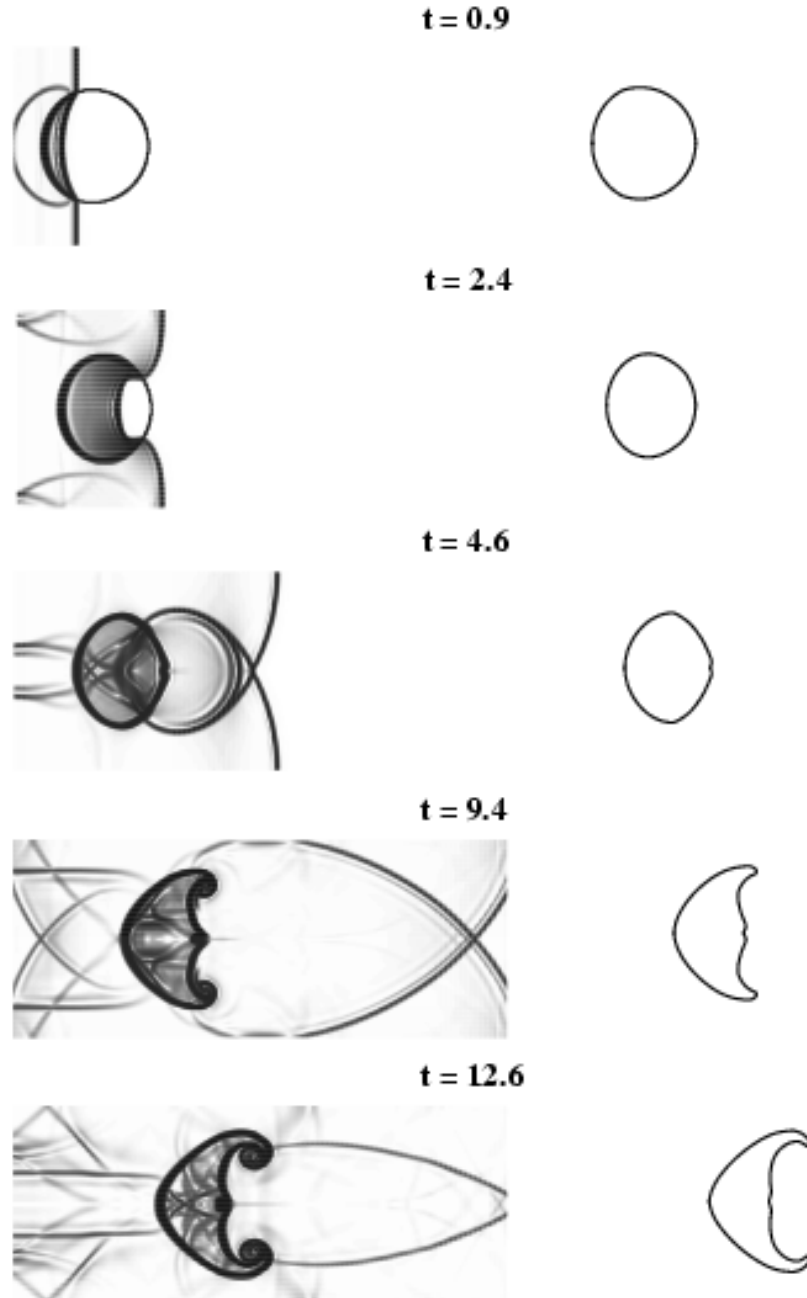


Figure 6 Normalized time sequence of numerical image (left) and interface (right) for $M = 1.2$ shock interaction with $R22$ bubble

It is found that the present numerical images for both light and heavy cylindrical bubbles show similar evolution of shock-bubble interaction found by the experiment [16] and

numerically performed using an unstructured adaptive grid [15]. However, a quantitative comparison is made by plotting distance-time variations for certain positions in the bubble interface such as upstream, downstream and jet. Figure 7 and 8 depict the distance-time curves for both light (*He*) and heavy (*R22*) bubble, respectively. The present results are compared with the experimental results of Haas and Sturtevant [16] and the numerical results of Quirk and Karni [15]. The present results show fairly good agreement.

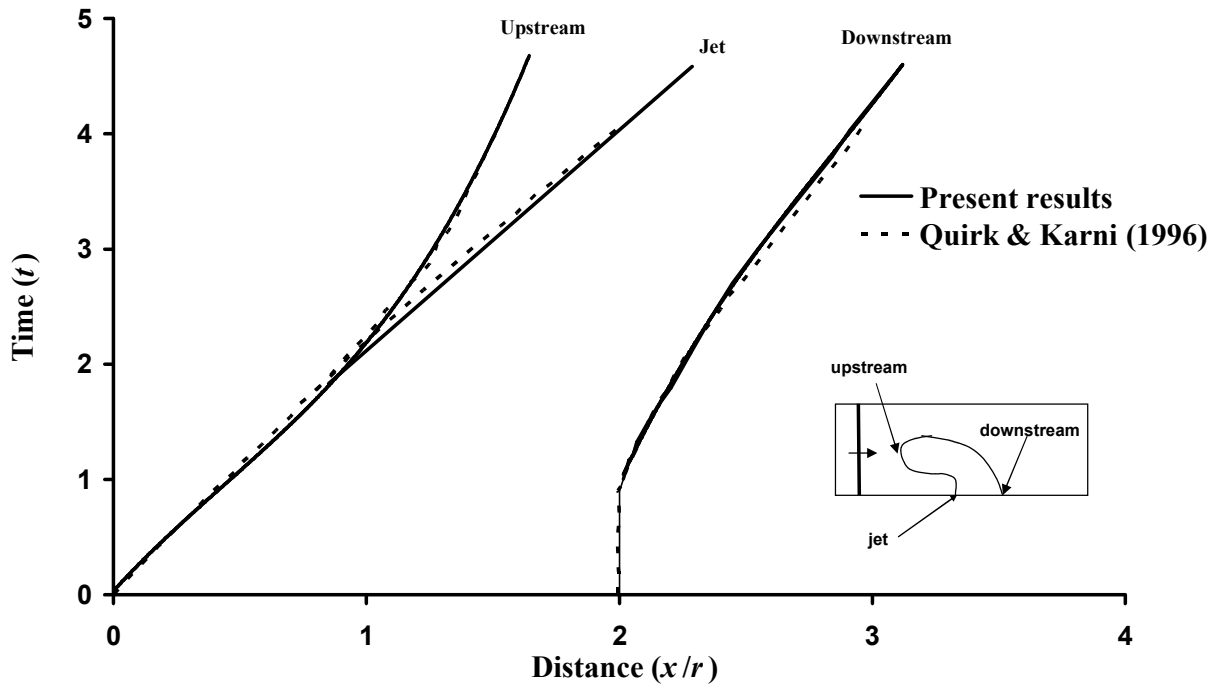


Figure 7 Distance-time plots at upstream, downstream and jet for $M = 1.2$ shock interaction with *He* bubble; comparison with the results of Quirk and Karni [15]

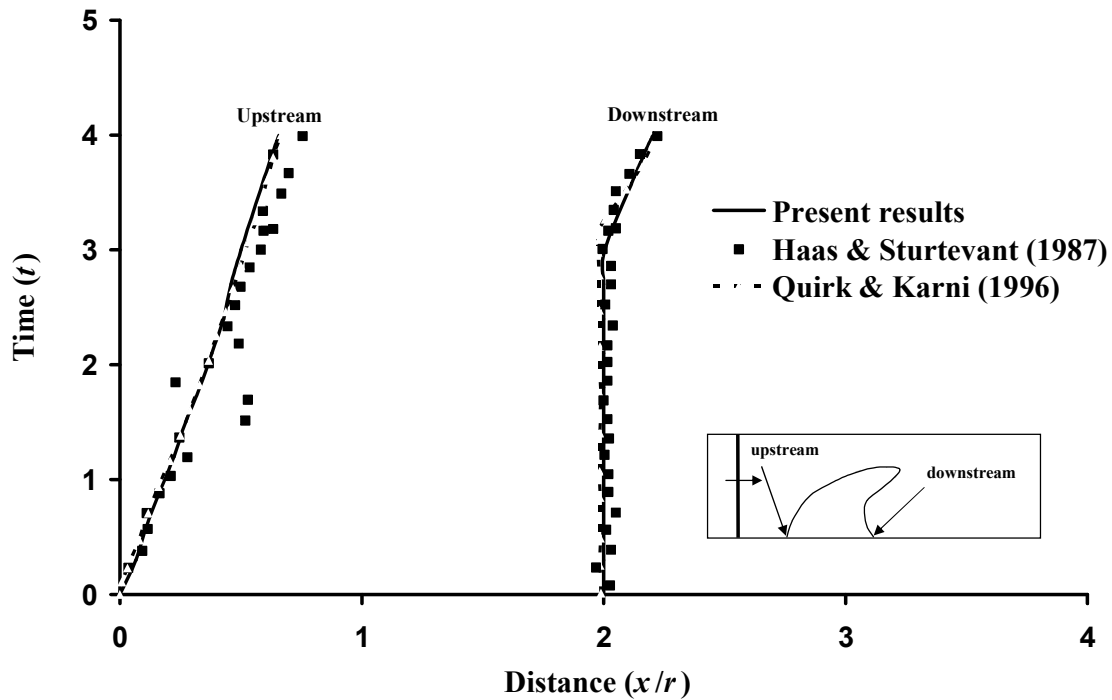


Figure 8 Distance-time plots at upstream and downstream for $M = 1.2$ shock interaction with *R22* bubble; comparison with the results of Haas and Sturtevant [16] and Quirk and Karni [15]

3.2 Air/ SF_6 sinusoidal interface

The experiment of Benjamin *et al.* [30] of Richtmyer-Meshkov instability is also here considered in order to evaluate the performance of the present solver. It consists of the evolution of a sinusoidal interface separating air and sulphur hexafluoride (SF_6). The test case has been utilised to compare full nonlinear numerical simulation of Zhang and Sohn [31] and Weaver *et al.* [32]. Consequently, extensive validated growth rate data is readily available. The initial configuration of the computational domain is depicted in Fig. 9. The experiment was conducted in a rectangular shock tube with an incident planar shock wave at Mach number of 1.2 which is initiated from the left-hand boundary. It travels from the air, with density 0.95 kg/m^3 , into SF_6 of density 4.85 kg/m^3 . Unshocked pressure in both gases is 0.8bar. The specific heat ratio of SF_6 is taken as $\gamma_{SF_6} = 1.09$. The sinusoidal interface is defined by the equation $x = a \cos\left(\frac{2\pi}{\lambda} z\right)$.

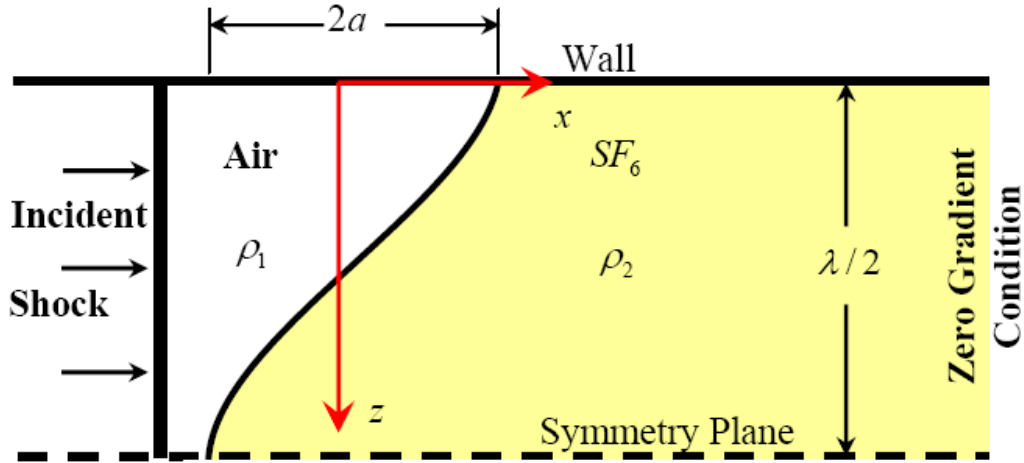


Figure 9 Schematic of computational domain of the sinusoidal interface

The initial amplitude, a , is taken as $2.4 \times 10^{-3} \text{ m}$ and the wavelength, λ , is $3.75 \times 10^{-2} \text{ m}$. Due to symmetry, the half wavelength solution is evaluated and a full wavelength solution is reconstructed about the symmetry plane to aid in visualisation, see Fig. 9. The test case is computed in 500×100 Cartesian grids.

Figure 10 shows the evolution of the sinusoidal interface at a sequence of time $T=0, 300, 500, \text{ and } 800$ microseconds (μs). The time $T=0$ corresponds to the first collision of the shock wave with the interface. The spike of the interface at the centreline of the shock tube is grown due to Richtmyer-Meshkov instability. It is noticed that the evolution of the sinusoidal interface obtained by the present numerical solver is similar to the past numerical studies [15].

A quantitative comparison of the growth rate history of the present numerical results with the experiment of Benjamin *et al.* [30] and previous numerical studies of Zhang and Sohn [31] and Weaver *et al.* [32] is plotted in Fig. 11. The growth rate is defined as $(u_{spike} - u_{bubble})/2$, where u_{spike} and u_{bubble} are the x -wise velocities at the extremities of the spike and bubble, respectively.

The exact locations of the spike and bubble are shown in Fig. 10. The present growth rate is recorded at every $0.7 \mu\text{s}$. This yields that the curve of the present results shown in Fig. 11 is represented by about 1100 points. In general, the present growth rate is fluctuated around the same value of the previous numerical studies. The deviation noticed between all numerical results and the experimental data of Benjamin *et al.* [30] may be due to the neglected viscous action, i.e. the boundary layer interaction with the shock wave in the duct. Another elucidation can be also here introduced in which non accurate measurements in supersonic flows.

It is obvious that the present calculations exhibit lower growth rate than the previous numerical studies between 150 and $240 \mu\text{s}$. It is worth mentioning that the grid test is performed for 1000×200 grid points without any noticeable change in the growth rate.

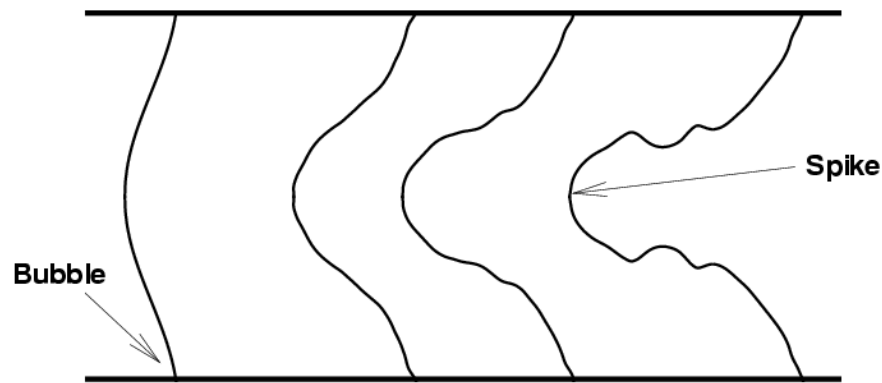


Figure 10 Evolution of the sinusoidal interface after interaction with shock at $M = 1.2$; The solutions are recorded at the time $T = 0, 300, 500,$ and $800 \mu s$ (from left to right)

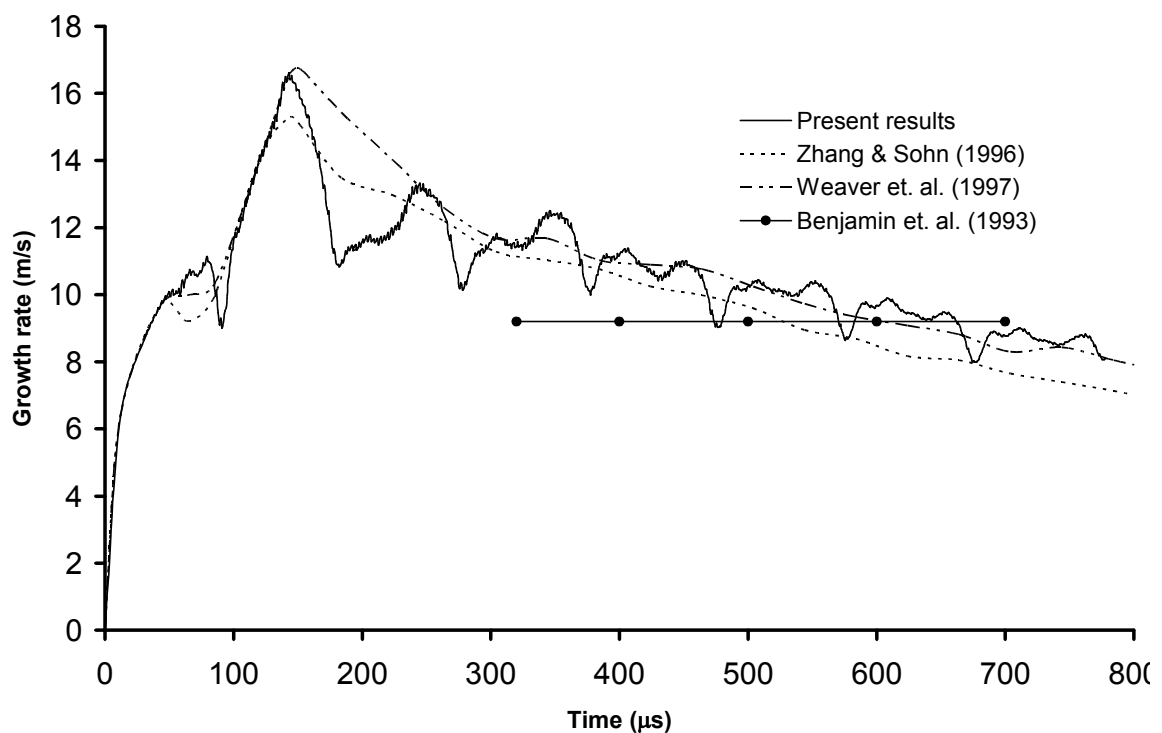


Figure 11 Growth rate history of the sinusoidal air/ SF_6 interface; comparisons with the results of Benjamin *et. al.* [30], Weaver *et. al.* [32] and Zhang and Sohn [31]

3.3 Air/He inclined interface

The final test case considered is the shock wave interaction with an inclined interface. As shown in Fig. 12, an incident planar shock wave at Mach number $M = 2$ is initiated from the left-hand boundary. It travels from the air into He gas. The density ratio of He to air is considered as $\rho_{He}/\rho_{air} = 0.166$. Unshocked pressure in both gases is considered to be 1.0 bar. The ratio of specific heats of He gas is $\gamma_{He} = 1.67$. The upper and lower boundaries of the domain are the wall of the shock tube. The test case is computed in 500×100 Cartesian grid points. The interface is inclined by an angle of $\theta = 45^\circ$ to the lower wall. However, this is only a pure numerical test case without experimental findings.

Figure 13 illustrates time sequence of numerical images (left) and the corresponding interface evolution (right) for shock interaction with air/ He inclined interface. The first frame is at time $T = 20 \mu s$ after the first shock-interface collision. The shock system is regular reflection, RR . The incident shock connects the interface with the curved refracted and reflected waves. The refracted

wave moves faster than the incident shock. At first frame, the bottom of the inclined interface starts to deform. At $T=50\mu s$, the shock system is changed to the twin regular reflection-refraction, TRR [2]. The circular vortical structure develops and interacts with the lower sides of the interface. About $\frac{3}{4}$ of interface has been deformed. At $T=100\mu s$, the incident shock is entirely transmitted from the air side and the interface is fully developed. The lower-circular vortical structure grows up and moves upwards. Also, another vortical structure near the upper wall starts to grow up. In the last two frames ($T=150-250\mu s$), the vortical structures are dominant resulting in a large distortion of the interface. On the other hand, the air side behind the interface exhibits many shock-shock interactions and shock focusing events.

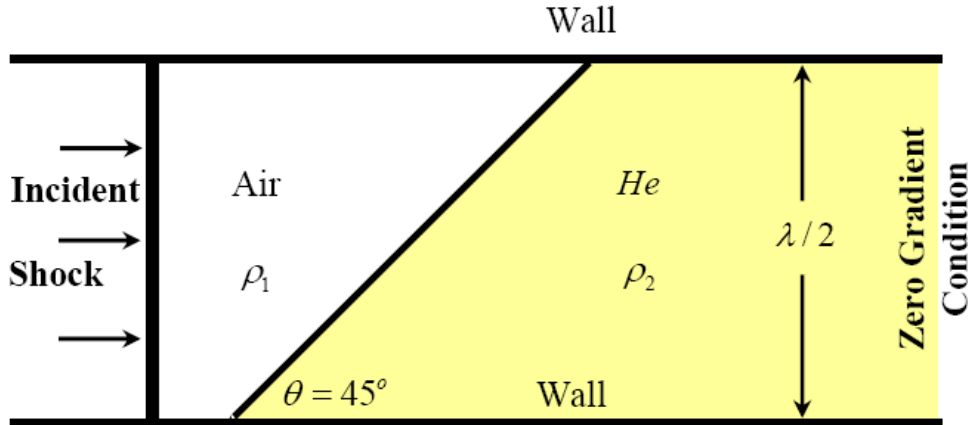


Figure 12 Schematic representation of the computational domain of the inclined interface

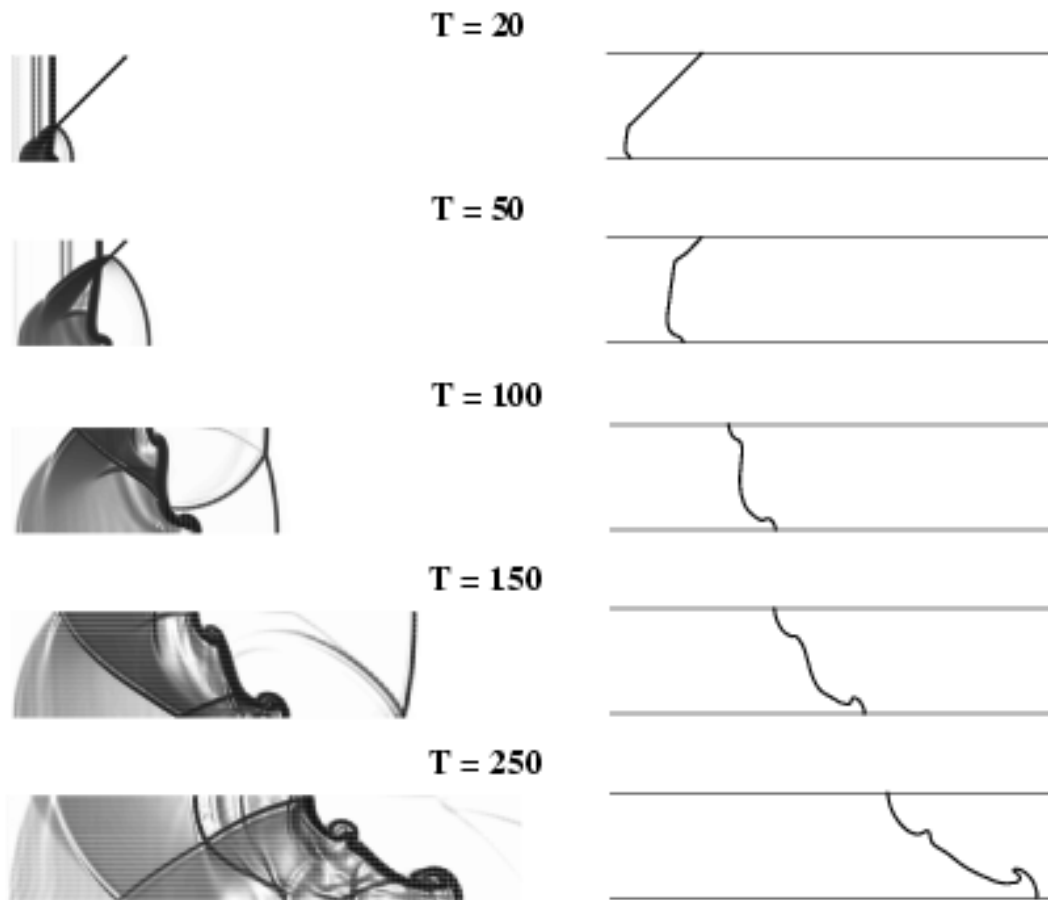


Figure 13 Normalized time sequence of numerical images (left) and interface evolution (right) for $M = 2$ shock interaction with air/He inclined interface. Time is in μs

4. Conclusion

The purpose of the present research was to perform a numerical study for the computation of two-gas flow along with a suitable and accurate surface tracking method. Consequently, a numerical simulation of compressible, two-gas flows using level set method was carried out to achieve better predictions of the physical processes occurring and to exclude some of the previous associated numerical instabilities. Implicit-unfactored unsteady hybrid Riemann solver using level set was presented and assessed. The performance of the solver was assessed through a series of numerical experiments of interaction of shock wave with cylindrical, sinusoidal and inclined interface separating two gases. All test cases were performed in 500×100 Cartesian grids. Firstly, the solver was validated against the experiments of Haas and Sturtevant [16] for a shock wave interaction with light (*He* gas) and dense (*R22* gas) cylindrical bubble. The numerical images for both bubbles showed good agreements with the past numerical [15] and experimental studies [16]. Furthermore, the velocities of the interface were well agreed with the past studies. The solver was also assessed for the experiment of Benjamin *et al.* [30]. It consists of evolution of a sinusoidal interface, separating air and sulphur hexafluoride (*SF₆*), due to shock interaction. It was revealed the present numerical solver produced similar interface evolution. The present interface growth rate was found similar to the previous numerical studies [31, 32]. However, it exhibited oscillation around the same value of the previous numerical studies. The final test case was $M=2$ for shock-wave interaction with 45° inclined interface separating air and *He* gas. The present numerical images revealed the fine details of the interface evolution and shock focusing event.

References

- [1] Cocchi J. P., Saurel R. A Riemann problem based method for the resolution of compressible multimaterial flows. *Journal of Computational Physics* 1997; 137:265-298.
- [2] Henderson L. F., Colella P., Pucker E. G. On the refraction of shock waves at a slow-fast gas interface. *Journal of Fluid Mechanics* 1991; 22(4):1-24.
- [3] Klein R. I., Colella P. The interaction of a supernova remnant with interstellar clouds using high order local adaptive mesh refinement methods. Lawrence Livermore National Laboratory, Livermore, California (USA); UCRL-100762 1989.
- [4] Taylor G. I. The instability of liquid surfaces when accelerated in a direction perpendicular to their plane. *Proc. Roy. Soc.* 1950; A210:192-196.
- [5] Richtmyer R. D. Taylor instability in shock acceleration of compressible fluids. *Comm. Pure Appl. Math.* 1960; 13:297-319.
- [6] Meshkov E. E. Instability of a shock wave accelerated interface between two gases. *Izv., Akad. Nauk SSSR, Mekh. Zhidk. I Gaz.* 1969; 151-158 (NASA translation TT F-13,074 R.F. (1970)).
- [7] Rupert V. Shock-interface interaction: Current research on the Richtmyer-Meshkov Problem. 18th International Symposium on Shock Waves, Sednai, Japan 1991; July 21-26.
- [8] Jenny P., Müller P., Thomann H. Correction of conservative Euler solver for gas mixtures, *Journal of Computational Physics* 1997; 132:91-107.
- [9] Karni S. Viscous shock profiles and primitive formulations. *SIAM Journal of Numerical Analysis* 1992; 29:1592-1609.
- [10] Karni S. Multicomponent flow calculations by a consistent primitive algorithm. *Journal of Computational Physics* 1994; 112:31-43.
- [11] Karni S. Hybrid multifluid algorithms. *SIAM Journal of Scientific Computing (SISC)* 1996; 17:1019-1039.
- [12] Shyue K. An efficient shock-capturing algorithm for compressible multi-component problems. *Journal of Computational Physics.* 1998; 142:208-242.
- [13] Qamar S., Warnecke G. Simulation of multi-component flows using high order central schemes. *Applied Numerical Mathematics* 2004; 50:183-201.

- [14] Xu K. Gas evolution dynamics in Godunov-type schemes and analysis of numerical shock instability. ICASE 1998; Report No. Tr. 99-6.
- [15] Quirk J. J., Karni S. On the dynamics of a shock-bubble interaction. *Journal of Fluid Mechanics* 1996; 318:129-163.
- [16] Haas J. F., Sturtevant B. Interaction of weak shock waves with cylindrical and spherical gas inhomogeneities. *Journal of Fluid Mechanics* 1987; 181:41-76.
- [17] Picone J. M., Boris J. P. Vorticity generation by shock propagation through bubbles in a gas. *Journal of Fluid Mechanics* 1988; 189:23-51.
- [18] Yang J., Kubota T., Zukoski E. E. Applications of shock-induced mixing to supersonic combustion. *AIAA Journal* 1993; 31:854-862.
- [19] Loehner R., Picone, J. M., Boris J. P. Wave structure produced by shock propagation through a dense bubble gas. In Proc. 16th Intl. Symp. on Shock Tubes and Waves, held at Aachen, Germany 1987. Edited by H. Gronig, Weinheim, Germany, 1988; 613-619.
- [20] Thornber B., Drikakis D., Youngs D. Large-eddy simulation of multi-component compressible turbulent flows using high resolution methods. *Computers & Fluids* 2008; 37:867-876.
- [21] El-Askary W. A. Turbulent boundary layer structure of flow over a smooth-curved ramp. *Computers & Fluids* 2009; 38:1718-1730
- [22] Mulder W., Osher S. J., Sethian J. A. Computing Interface Motion in Compressible Gas Dynamics. *Journal Computational Physics* 1992; 100:209-228.
- [23] Karni S. A level-set scheme for compressible interfaces. *Numerical Methods for Wave Propagation*, Kluwer Academic Publishers, Dordrecht. 1988; 253-274.
- [24] Abgrall R., Karni S. Computation of compressible multi-fluids. *Journal of Computational Physics* 1991; 169:594-623.
- [25] Wang C., Tang H., Liu T. An adaptive ghost fluid finite volume method for compressible gas-water simulations. *Journal of Computational Physics* 2008; 227:6385-6409.
- [26] Abgrall, R. Generalisation of the Roe scheme for the computation of mixture of perfect gases. *La Recherche Aeronautique* 1988; 6,:31-43.
- [27] Lax, P. D. Weak solutions of nonlinear hyperbolic equations and their numerical computation. *Comm. Pure Appl. Math.* 1954; 7:159-163.
- [28] Lax, P. D., *Hyperbolic systems of conservation laws and the mathematical theory of shock waves*. SIAM Monograph series 1972.
- [29] Quirk, J. J., An adaptive mesh refinement algorithm for computational shock hydrodynamics. PhD Thesis, Cranfield Institute of Technology, U.K., 1991.
- [30] Benjamin R., Besnard D., Haas J. F. Shock and reshock of an unstable interface. LANL Report LA-UR 92-1185, Los Alamos National Laboratory 1993.
- [31] Zhang Q., Sohn S. An analytical theory of Richtmyer-Meshkov instability. *Physics Letters A* 1996; 212:149-155.
- [32] Weaver R. P., Gittings M. L., Baltrusaitis R. M., Zhang Q., Sohn S. 2D and 3D simulations of RM instability growth with RAGE: A continuous adaptive mesh refinement code. Proceedings of the 21st International Symposium on Shock Wave 1997, Great Keppel Island, Australia, July 20-25, 1997.
- [33] Bagabir A., Drikakis D. Shock-diffraction phenomena and coherent structures during the interaction of a shock wave with a bubble. In Ball and Hillier and Roberts (editors), *Proceeding of 22nd International Symposium on Shock Waves* 1999; 2:1059-1064, Imperial College, London, United Kingdom (1999)
- [34] Bagabir A., Drikakis D. A comparative study of implicit HLL, HLLC and hybrid Riemann solvers in unsteady compressible flows. In: Toro EF (ed.) *Godunov Methods: Theory and Applications*. Kluwer Academic/Plenum Publishers 2001.
- [35] Bagabir A., Drikakis D. Numerical experiments using high-resolution schemes for unsteady, inviscid, compressible flows. *Computer Methods in Applied Mechanics and Engineering* 2004; 193:4675-4705.

- [36] Eberle A. Characteristic flux averaging approach to the solution of Euler's equations. VKI Lecture Series, Computational Fluid Dynamics 1987; 1987-04.
- [37] Drikakis D. and Tsangaris S. On the solution of the compressible Navier-Stokes equations using improved flux vector splitting methods. *App. Math. Modelling* 1993; 17:282-297.
- [38] Eberle A., Rizzi and Hirschel E. Numerical solutions of the Euler equations for steady flow problems. *Notes on Numerical Fluid Mechanics* 1992; 34, Vieweg Verlag.
- [39] van Albada G., van Leer B., Roberts W. Comparative study of computational methods in cosmic gas dynamics. *Astron. Astrophys* 1982; 108.
- [40] Thomas J., van Leer L., Walters B. Implicit flux split scheme for the Euler equations. AIAA-paper 85-1680; 1985.
- [41] Chakravarthy S. R. Relaxation methods for unfactored implicit upwind schemes. AIAA-84-0165; 1984.
- [42] Sethian J. A. *Level Set Methods: Evolving interfaces in geometry. Fluid Mechanics, Computer Vision and Materials Sciences*, Cambridge Univ. Press. 1st ed. 1996.
- [43] Sussman M., Smereka P., Osher S. A Level set approach for computing solutions to incompressible two-phase flow. *Journal of Computational Physics* 1994; 114-146.
- [44] Balabel A., Binninger B., Herrmann M., Peters N. Calculation of droplet deformation by surface tension effects using the level set method. *Journal of Combustion Science and Technology* 2002; 174:257-278.
- [45] Sethian J. *Level set methods*. Cambridge University Press. 1996.